Automatic Orthorectification of High-Resolution Optical Satellite Images Using Vector Roads

Aleš Marsetič, Krištof Oštir, and Mojca Kosmatin Fras

***Abstract*—This paper presents a completely automatic processing chain for orthorectification of optical pushbroom sensors. The procedure is robust and works without manual intervention from raw satellite image to orthoimage. It is modularly divided in four main steps: metadata extraction, automatic ground control point (GCP) extraction, geometric modeling, and orthorectification. The GCP extraction step uses georeferenced vector roads as a reference and produces a file with a list of points and their accuracy estimation. The physical geometric model is based on collinearity equations and works with sensor-corrected (level 1) optical satellite images. It models the sensor position and attitude with second-order piecewise polynomials depending on the acquisition time. The exterior orientation parameters are estimated in a least squares adjustment, employing random sample consensus and robust estimation algorithms for the removal of erroneous points and fine-tuning of the results. The images are finally orthorectified using a digital elevation model and positioned in a national coordinate system. The usability of the method is presented by testing three RapidEye images of regions with different terrain configurations. Several tests were carried out to verify the efficiency of the procedure and to make it more robust. Using the geometric model, subpixel accuracy on independent check points was achieved, and positional accuracy of orthoimages was around one pixel. The proposed procedure is general and can be easily adapted to various sensors.**

***Index Terms*—Automatic orthorectification, general physical geometric model, ground control point (GCP) extraction, optical imagery, random sample consensus (RANSAC), RapidEye, robust estimation.**

I. Introduction

In THE last decades, many Earth observation satellites of all sizes and capabilities have been launched to image Earth's surface for various applications. The data amount and the availability of remotely sensed images are increasing and becoming accessible to many scientists and entrepreneurs. Several satellite images have medium (100–10 m), high (10–1 m), or very high (1 m and below) spatial resolution and, if properly prepared, are very valuable in applications where high positional precision is required. Sometimes, users need very high accuracy for low-resolution images (300 m or more), as well as on rough terrain with high mountains. To achieve this kind of precision independently on the terrain configuration, users demand geometrically preprocessed data, i.e., images free of geometric distortions caused by topography, Earth curvature, sensor errors, and satellite viewing angle, and georeferenced to known cartographic reference systems. Furthermore, in some applications, geometrically preprocessed images must be available in near real time. The need for a robust—automatic and generic—procedure for image orthorectification is therefore huge.

Almost all state-of-the-art high-resolution optical satellites utilize linear scanners that acquire one line at a time. In this case, the geometry and acquisition mode is complex, and every line has its own exterior orientation elements (position and attitude). Although satellites have advanced attitude determination systems (e.g., star trackers) and positioning systems (e.g., Global Positioning System receivers), their accuracy is still not sufficient for direct georeferencing of images [1] in applications where high precision is required. This shortcoming can be resolved by means of indirect methods, which utilize ground control points (GCPs). GCP collection requires major effort as they are usually obtained manually or semiautomatically. Process automatization is difficult and often produces undesired results in the form of erroneous or badly distributed GCPs. In some cases, automatic GCP extraction produces a certain amount of very accurate points, but they are then hard to filter and separate from the erroneous ones, which usually contain gross errors (blunders). Only an efficient "seek-and-remove" method can clean the automatically generated set of points and contribute to an accurate geometric model parameters determination, which is a prerequisite for orthoimages that can be used in different applications, including geographic information systems.

Several automatic image registration methods for geometric correction of different sensors have been recently developed (e.g., [2]–[9]). Methods for optical satellite images are usually based on the extraction of GCPs from raw and reference data. These point pairs are then used in a geometric model (transformation), which corrects and aligns the raw image to the reference data. The efficiency of GCP extraction mostly depends on reference data and extraction algorithm, whereas

Manuscript received December 10, 2014; revised February 12, 2015 and March 11, 2015; accepted April 10, 2015. This work was supported by the Slovenian Centre of Excellence for Space Sciences and Technologies Space-SI, which was an operation partly financed by the European Union; the European Regional Development Fund; and the Ministry of Education, Science and Sport of the Republic of Slovenia.

A. Marsetič is with the Institute of Anthropological and Spatial Studies, Research Center of the Slovenian Academy of Sciences and Arts, 1000 Ljubljana, Slovenia (e-mail: ales.marsetic@zrc-sazu.si).

K. Oštir is with the Faculty of Civil and Geodetic Engineering, University of Ljubljana, SI-1000 Ljubljana, Slovenia, with the Institute of Anthropological and Spatial Studies, Research Center of the Slovenian Academy of Sciences and Arts, SI-1000 Ljubljana, Slovenia, and also with the Slovenian Centre of Excellence for Space Sciences and Technologies Space-SI, SI-1000 Ljubljana, Slovenia (e-mail: kristof@zrc-sazu.si).

M. Kosmatin Fras is with the Faculty of Civil and Geodetic Engineering, University of Ljubljana, SI-1000 Ljubljana, Slovenia (e-mail: Mojca.Kosmatin-Fras@fgg.uni-lj.si).

Color versions of one or more of the figures in this paper are available online at http://ieeexplore.ieee.org.

Digital Object Identifier 10.1109/TGRS.2015.2431434

geometric transformation can be performed with various functions [10]. The transformation function is based on the type of geometric distortion present in the image, its level of processing, and the available image metadata. Although many modern satellite images are equipped with rational polynomial coefficients (RPCs) [11], which are currently predominantly used for geometric corrections, they are not always optimal and are often less accurate than a rigorous model. In addition to the transformation function, the final orthoimage accuracy heavily depends on the precision of automatically extracted GCPs. Some automatic solutions for erroneous GCP removal (e.g., [12]) rely only on the data snooping method [13], which is not the optimal method, as it tends to fail when data with large errors and many gross errors are involved in the adjustment [14]. In these cases, more robust methods must be used.

The need to develop an automatic orthorectification processing chain emerged from the extensive automatic image processing methodology [15] developed by the Centre of Excellence Space-SI. This methodology was designed to work with many satellite systems and, in particular, the Slovenian small satellite [16], which is currently in the integration phase. The developed system produces radiometrically corrected orthoimages and normalized difference vegetation index based products. The automatically generated products can serve in many applications, for example, to update topographic databases or in other near-real-time applications. To satisfy the accuracy that is required in these applications, the goal was to produce a system that generates orthoimages with positional accuracy of the image pixel size or better.

This paper describes a completely automated production chain for generating orthorectified sensor-corrected (often denoted as level 1a and named as raw or input images in the rest of this paper) pushbroom satellite images. It addresses the challenges in the development phase and presents tests that were performed to assure robustness of the process. The algorithm was developed mostly in IDL, with some parts in C++, and the processing chain is divided in four main modules: metadata extraction, GCP extraction, geometric modeling, and orthorectification. They are managed by a Java control module, which also controls the image database. The first module performs automatic GCP extraction with vector roads as a reference. The module is written in C++ and can function as a stand-alone program. The file with the extracted GCPs is passed to the sensor geometric model. The geometric model is rigorous and exactly models the acquisition geometry of the sensor. Its efficiency was tested with a different number and distribution of GCPs and with artificially introduced gross errors to obtain an optimal version that produces accurate results as fast as possible. A very important feature is gross error removal as the automatic GCP extraction module can produce inaccurate points that may influence the outcome of the process. The affected points are treated by random sample consensus (RANSAC) and robust estimation methods. Since the choice of the optimal method is not trivial, a test for the selection of the best method was undertaken as well. The last module uses a digital elevation model (DEM) and estimated exterior orientation parameters to generate orthorectified images. Since only one image was processed at a time and an exact digital building model (DBM) was unavailable, orthorectification was only used to correct the effects of the terrain. The creation of true orthoimages [17] was thus outside the scope of this research.

The procedure is generic and can basically accommodate any pushbroom sensor with some adaptation. In the frame of the project, the procedure was tested on RapidEye, WorldView-2, Pleiades, SPOT 6, and THEOS images. However, in this paper, we focus on the processing of RapidEye images that were most extensively used and the first available during the development of algorithms. All images come with a metadata file in Extensible Markup Language (XML) format from where all information needed for the procedure is extracted. The entire processing, from the metadata extraction to the orthorectification in the national system, is fully automatic and does not require any manual intervention.

This paper is composed of three main sections. In the introduction, we present the background and motivation of our research. In the second section, the steps of the implemented automatic chain are presented in more details. The third section describes the empirical tests performed to verify the performance, robustness, and stability of the procedure and discusses the results. The fourth section summarizes the conclusions.

II. Automatic Orthorectification Chain

The automatic orthorectification procedure is divided into different steps (see Fig. 1). Some of them are tightly connected and work in iterations (geometric modeling and gross error removal), whereas others are mostly independent (e.g., GCP extraction) and could work as stand-alone modules. The chain is completely automatic, and the start of the processing can be triggered by the appearance of an image in a specifically designated folder on the processing server. At the moment of arrival, the process first starts with the extraction of useful information from the metadata file. The procedure then continues with GCP extraction, geometric modeling, and, finally, orthorectification. The final results are orthoimages and a log file with information about the processing, parameter values, and achieved accuracies.

A. Metadata Extraction and Preparation

Image metadata is important when it comes to any type of imagery processing, but it is essential in the geometric preprocessing step of pushbroom sensors with their complex geometry of acquisition. For orthorectification, at least the extraction of RPCs is required. However, when RPCs are not available or the sensor is rigorously modeled, various types of information about the orbit and the camera have to be extracted from the metadata file.

Metadata can have various file formats, which depend on the image provider. Traditionally, the files were in ASCII format, but in the last years, the tendency of the providers has been to supply metadata in an XML format file. The XML file is typically bigger and more complex than the ASCII file, but its structure makes it straightforward for reading and displaying in designated software.

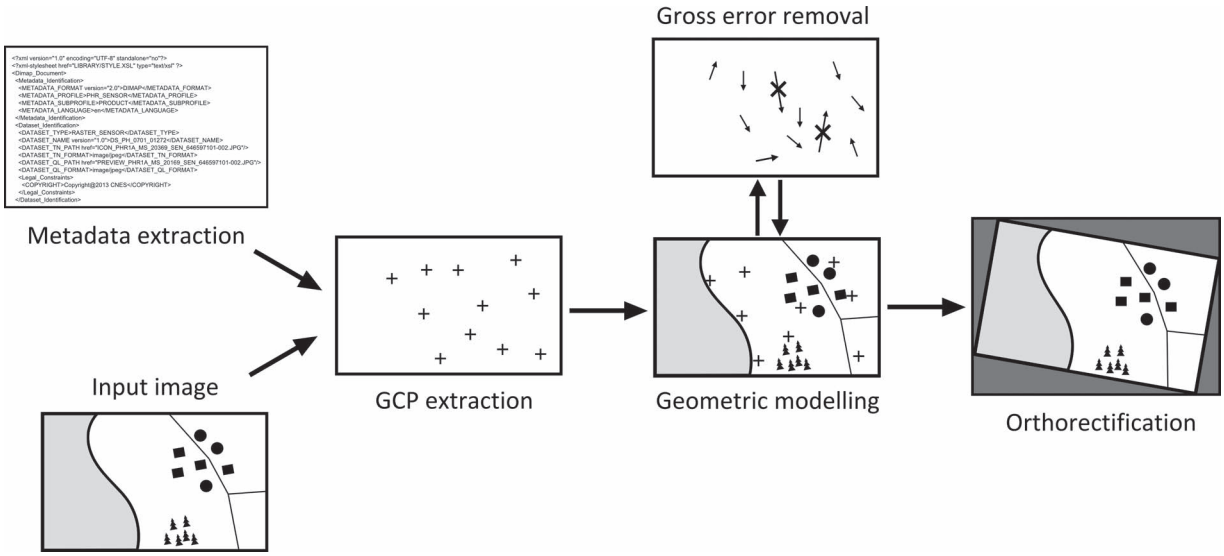

Fig. 1. Proposed automatic orthorectification chain. Different steps are needed to generate the orthoimage.

The developed automatic chain uses an XML file parser, which automatically extracts the specified parameters from the metadata file. The reader searches for predefined tags and saves the found values in specific variables stored in a structure with different data types. The parser extracts data about the sensor, image properties, and initial values of exterior orientation parameters. The extracted metadata values for RapidEye images are as follows:

1) image rows;
2) image columns;
3) image bands;
4) instrument focal length;
5) sensor pixel pitch;
6) satellite view angle;
7) date and time of acquisition;
8) first line time;
9) rotation of the platform;
10) position of the platform;
11) velocity of the platform.

The rotation, position, and velocity of the platform (satellite) are given for every second. The positions and speeds are in the Earth Centered Rotational (ECR) system, and the attitude is described by the roll, pitch, and yaw angles.

The extracted metadata is an input for the next modules. However, before it can be used in the geometric model, the initial values of the exterior orientation parameters must be transformed in the coordinate system of the model, which is also the final system of the orthoimage. The initial rotations and positions of the platform enter the model as approximate values of the exterior orientation parameters, which are finally determined in the geometric model.

The data preparation procedure first transforms the coordinates of the positions from the ECR system to the desired (e.g., national) system. As the coordinates are given for every second before, between, and after the acquisition, they are interpolated with cubic splines to best fit the measurements. From the interpolated values, the position of every image line can be easily determined.

Many modern satellite systems provide rotations in the form of quaternions; however, the rotations for RapidEye images are given relative to the orbit of the satellite (roll, pitch, yaw). To obtain the rotations in the desired local coordinate system, various transformations are required. First, the values are interpolated with cubic splines. Then, the interpolated values are rotated to the local system with the use of interpolated velocity vectors. The final rotations are obtained with the following equations [18]:

$$\begin{aligned} \omega &= a\tan\left(-\frac{r_{23}}{r_{33}}\right) \\ \phi &= a\sin(r_{13}) \\ \kappa &= a\tan\left(-\frac{r_{12}}{r_{11}}\right) \end{aligned} \tag{1}$$

where r_{xy} are the elements of the final rotation matrix.

All prepared data and other useful information extracted from the metadata file are stored and passed to the geometric modeling module.

B. GCP Extraction

Another input to the geometric model are the GCPs, which play a crucial role in the proposed chain. The accuracy of the extracted GCPs is very important and has a strong influence on the final results. Automatic GCP extraction from two different image data sources is a very difficult task due to the temporal variability of objects and different characteristics of the images involved. Traditional point-based and area-based methods that compute local similarity in image intensities (e.g., SURF and SIFT) were developed to coregister raw and reference images, but they often fail when working with multitemporal or multisensor images [19], [20].

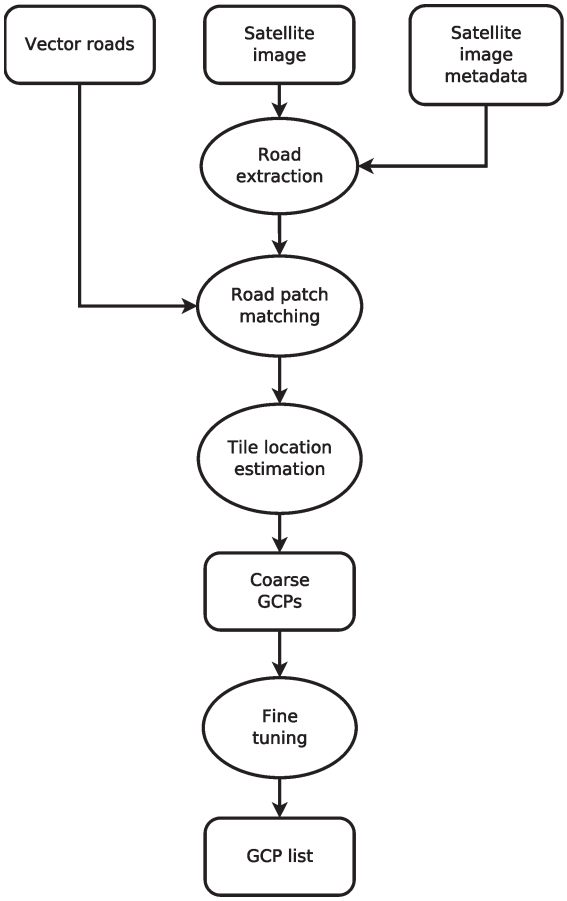

Fig. 2. Automatic GCP extraction module developed by Zaletelj *et al.* [21].

For this reason, we concentrated on vector data sets of roads, which are nowadays available almost everywhere in the world. Roads are usually a very stable and prominent structure and are easily detected on satellite images of different spatial resolutions. Additionally, road features lie on Earth's surface and are usually used as reference when GCPs are manually selected. The proposed automatic GCP extraction algorithm [21] (see Fig. 2) was developed within the Centre of Excellence Space-SI. The algorithm was written in C++ and performs matching of detected roads from satellite images to rasterized vector roads.

Before roads are extracted from the input (raw) image, clouds (if present) are removed. The cloud mask is generated by thresholding the high radiometric values on the histogram or is taken from the metadata if available. Then, the road detection is performed based on the morphological image filtering, using the top-hat morphological operator of a predefined size. The optimal width of the operator was selected dependent on the spatial resolution of the satellite images. The goal is to emphasize image areas of a predefined fixed width, which are brighter than the surrounding pixels, and, at the same time, to suppress image edges. The reference road layer consists of the rasterized national road database for Slovenia, complemented with the rasterized OpenStreetMap for the neighboring countries.

To simplify the processing, the input data are tiled based on their size. The road image is transformed to road distance image, resulting in pixel values corresponding to the distance to the closest road pixel. Then, the GCP retrieval process is performed in a few steps. The first step performs coarse registration of satellite image tiles, resulting in a set of perspective transform parameters, which relate coordinates of the resampled satellite tile image pixels and road distance image pixels. The nine parameters are calculated from a valid set (approximately 20) of equally spaced point pairs with coordinates $t_k = [x_k^{(t)}, y_k^{(t)}]$. The predicted position within the road image is $r_k = [x_k^{(r)}, y_k^{(r)}]$. Their position is determined by computing the match between detected satellite roads and the road distance image within a search region and selecting the best matching positions as probable point coordinates. The correlation between the patch from the detected roads image, i.e., P, and the road distance image, i.e., D, is computed for each possible position within the search region centered at r_k. This road matching criterion gives an average distance of satellite road pixel to the closest reference road pixel at the specified position Δ within the search region around the predicted position r_k. The proposed criterion is given by the following equation:

$$C(r_k + \Delta) = \frac{1}{N_R} \cdot \sum_{x=0}^{s_x} \sum_{j=0}^{s_y} P\left(x_k^{(t)} + x, y_k^{(t)} + y\right) \cdot D\left(x_k^{(r)} + \Delta_x + x, y_k^{(r)} + \Delta_y + y\right) \quad (2)$$

where N_R is the number of road pixels within the road patch, and s_x, s_y is the size of the patch in the x and y directions.

Within this search area, many local minima of the criteria appear that are obtained by matching detected roads with the reference roads. For each sample point, we select a few best matching positions Δ as candidate point locations. The final matching candidate is selected by minimizing the correlation-based distance. This step ends with a validation against the known initial tile position, scaling, and rotation. If the tile does not fall within the accuracy thresholds, it is removed; otherwise, the second step begins.

First, a suitable number of candidate GCPs per each tile are selected according to the perspective transformation. The selected points must fulfill the requirement of lying on road intersections that are obtained from the vector roads layer. Then, the optimized final location of the GCPs is found as the minimum of the road match criterion (local minimum of distances between the reference and extracted road sections) within a smaller search radio. The procedure uses a variation of (2). Fig. 3 shows the final position of a GCP on a road intersection of detected roads with the road distance image in the background. The final GCP selection is done through quality assessment with an average road distance criterion (distance to the closest road averaged over all detected road pixels) within the search area. By setting a suitable threshold on this criterion, outliers can be removed, and the point errors can be additionally minimized.

After the final step, an ASCII file is generated with the list of selected GCPs with pixel coordinates, map coordinates, and their quality based on the average road distance criterion. The rough number of points can be determined before the module starts, but is limited by the number of available road sections.

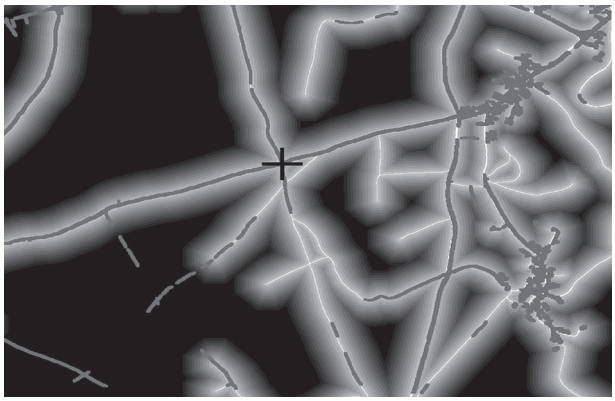

Fig. 3. Selected GCP on the detected road patch (intersection) registered on the road distance image in the background.

The preliminary results show that subpixel GCP accuracy (RMS error) can be achieved if compared with bias-corrected RPC coordinates [21].

C. Geometric Modeling

The extracted GCPs serve as an input to the geometric modeling module (see Fig. 4). Currently, the module works with images acquired by pushbroom sensors and at sensor-corrected level. It can basically work with every linear array sensor with supplied metadata about the sensor characteristics and line acquisition times with approximate position and attitude (ephemerides). The implemented generic geometric model is intended to work with only one image at a time to streamline the processing when orthorectified images are needed in a very short time.

The geometric model is physical or rigorous, which means that it models the viewing geometry of the sensor at the time of the image acquisition. The relationship between the sensor and the ground coordinate system is represented by the collinearity equations. Because the interior orientation parameters of modern satellites are normally very stable [22], the geometric model computes only the exterior orientation parameters, whereas the interior parameters are taken from the results of laboratory calibrations that are usually found in the metadata file.

The exterior orientation parameters are modeled by time-dependant piecewise polynomial functions. During processing, the satellite orbit is divided into two segments, which is optimal for most satellite sensors [1]. In each segment, the sensor exterior orientation is modeled by six equations with 12 parameters (three for each coordinate and one for each rotation), where three second-order polynomial equations depend on time t. The equations have constant $(X_0, Y_0, Z_0, \omega_0, \varphi_0, \kappa_0)$, linear (X_1, Y_1, Z_1), and quadratic (X_2, Y_2, Z_2) terms, i.e.,

$$\begin{aligned} X(t) &= X_0 + X_1\, t + X_2\, t^2 \\ Y(t) &= Y_0 + Y_1\, t + Y_2\, t^2 \\ Z(t) &= Z_0 + Z_1\, t + Z_2\, t^2 \\ \omega &= \omega_0 \\ \phi &= \phi_0 \\ \kappa &= \kappa_0. \end{aligned} \tag{3}$$

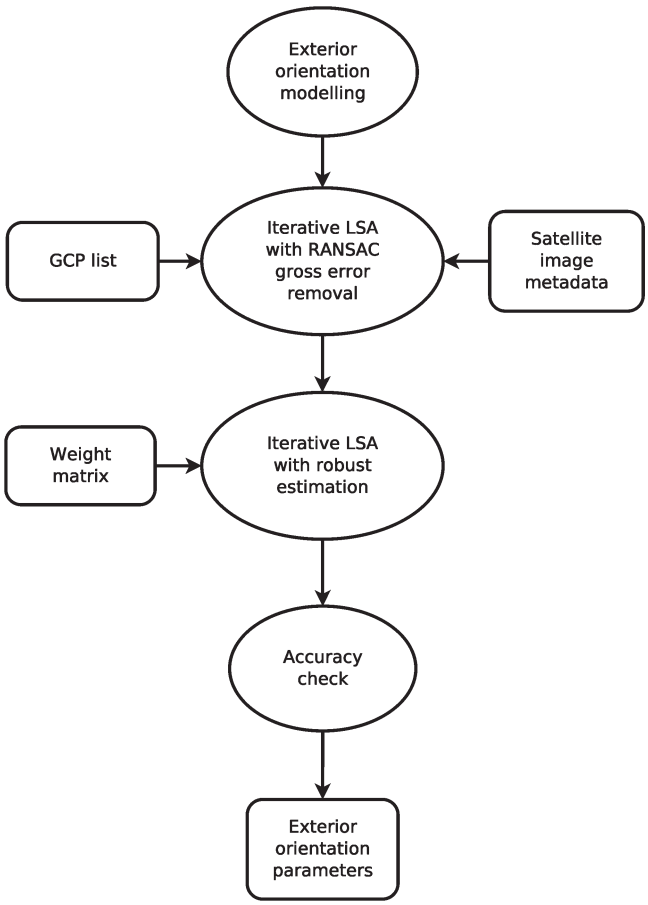

Fig. 4. Geometric modeling module.

The attitude parameters are treated as constants as they do not change significantly during the image acquisition. The smoothness of the orbit at the point of conjunction between adjacent segments is obtained with constraining the zeroth-, first-, and second-order continuity (derivatives) on the orbit functions.

The model is solved with a least squares adjustment (LSA) utilizing automatically extracted GCPs. Because the number of unknowns for one image is 24 (12 unknowns for each of the two segments), at least six GCPs are required for the solution of the equation system (each GCP gives two observation equations, whereas the constraints on the continuity of the orbit functions give 12 additional equations). However, more points are recommended to increase the redundancy. Before the iterative adjustment, the GCPs coordinates are corrected for systematic errors that include the effect of Earth curvature and atmospheric refraction [23]. The weights of the GCPs are calculated based on their quality that was computed during their extraction. In each adjustment iteration, the exterior orientation parameters are estimated, and the GCP coordinate corrections are calculated. For the internal accuracy, the sigma naught a posteriori and the RMS error of the GCP coordinates are computed. These values are then supplied to the gross error detection algorithms that are implemented in the geometric model and described in the following section.

D. Gross Error Removal

Because the GCPs are automatically extracted and their quality cannot be checked visually, some points may have coordinates that are burdened with gross errors. These GCPs may have a considerable influence on final results if their effect is not minimized or removed. The geometric model can be used to find these points, remove them, or just reduce their effect.

To remove the effect of gross errors on the final exterior orientation parameters, the implemented geometric model works in two stages. In the first one, the GCPs with large gross errors are removed by means of the RANSAC algorithm [24]. RANSAC is an iterative method, which estimates the parameters of a mathematical model from observations that usually include errors. It is reliable even when a large number of gross errors are present in the observations (up to 40%), in which case some other methods, e.g., data snooping, usually fail. As an iterative method, the process can be time consuming, particularly if many gross errors are present. This first stage is divided into two parts, where the first one selects the points that best fit the initial solution. If the number of points does not meet the empirically determined threshold, the parameter governing the maximum point error is increased by a predefined value (half pixel), and the iteration is repeated. When the threshold is reached, the second phase computes the exterior orientation parameters and the a posteriori standard deviation via a least squares adjustment. The processing continues until a predefined number of iterations is reached, and the solution with the smallest standard deviation is stored for the second stage.

The second stage works only with the points that were not removed in the first stage. These points have small errors and are harder to identify in an automatic way. Their effect to the adjustment results can be reduced with the use of robust estimation methods. In photogrammetry, the robust estimation started to be utilized in the 1980s [25], whereas the idea was already formed in the 1960s [26]. In contrast to the least squares method, robust estimation does not minimize the square error, but uses the chosen weight function. In photogrammetry, the weight function is used to calculate the weights of the observations after every adjustment iteration according to their accuracy. This means that the observations with larger residuals receive a smaller weight, which reduces their influence in the adjustment results. The weight function can have different forms, and in the past, various methods were developed. In this paper, three approaches were tested: the Danish method [25], the method of Klein [27], and a simple hyperbolic function. The Danish method uses an exponential weight function, and in our case, the weight was computed with

$$P_i = \exp\left(-\frac{r_i^2}{(2\sigma)^2}\right) \tag{4}$$

where P_i is the new weight, r_i is the residual, and σ is the standard deviation. The method of Klein works with a hyperbolic function

$$P_i = P_j \frac{1}{1 + (a_i \cdot |r_i|)^d} \tag{5}$$

in which

$$a_i = \frac{\sqrt{P_j}}{4.4 \cdot \sqrt{\mathrm{or}} \cdot \sigma}$$
$$d = 3.5 + \frac{82}{81 + Q^4}$$
$$Q = \frac{\sigma}{\sigma_{\mathrm{a-priori}}}$$

and or is the observation redundancy. The last method tested was computed with the hyperbolic function

$$P_i = \frac{1}{1 + \frac{|r_i|}{\sigma}}. \tag{6}$$

The initial weights are formed using the GCPs quality, which was calculated during the GCPs extraction. If during the adjustment iteration the residual of a point is above the specified threshold (which is empirically set to 2σ), its weight is reduced based on the error function. The process is repeated until all residuals are within the threshold. This way, all GCPs are retained, but their influence on the computation of the final orientation parameters is limited. The final internal accuracy is determined by the sigma naught a posteriori, whereas the external accuracy on check points cannot be asserted at this stage of the automatic process.

E. Orthorectification

The last part of the processing chain generates orthoimages. The scope of the presented research was to quickly generate orthoimages from high and very high resolution (VHR) images with the available DEMs to correct the effects of the terrain. As some studies suggest (e.g., [17], [28]), generation of true orthoimages can improve the interpretability and exactness of the products, particularly in urban areas. To achieve this kind of product, the use of multiple images (to avoid occlusions) and an accurate DBM is required. Since the production chain works with one image at a time and since we did not have a suitable DBM, this study was limited to the generation of terrain-corrected orthoimages.

Orthorectification requires a DEM or a digital surface model (DSM) and uses collinearity equations to rigorously project the pixels from the input image to the orthoimage. In general, there are two groups of orthorectification methods. The first group includes direct methods that project the pixels from the raw image to the object space [29]. Direct methods function with an iterative process and can be very precise in combination with a very accurate DSM. The drawback of these iterative methods is the longer processing times, particularly in regions with rough terrain. The procedures of direct orthoimage generation may result in orthoimage pixels with unassigned gray values. Therefore, the missing gray values must be interpolated from neighboring pixels. When working with VHR imagery and very detailed DSMs, the empty pixels may form significant occlusions, which are hard to fill without additional images. Some of these methods can be also used for true orthophoto generation. The second group, the so-called indirect methods (see Fig. 5), works in the opposite direction. These methods start in the

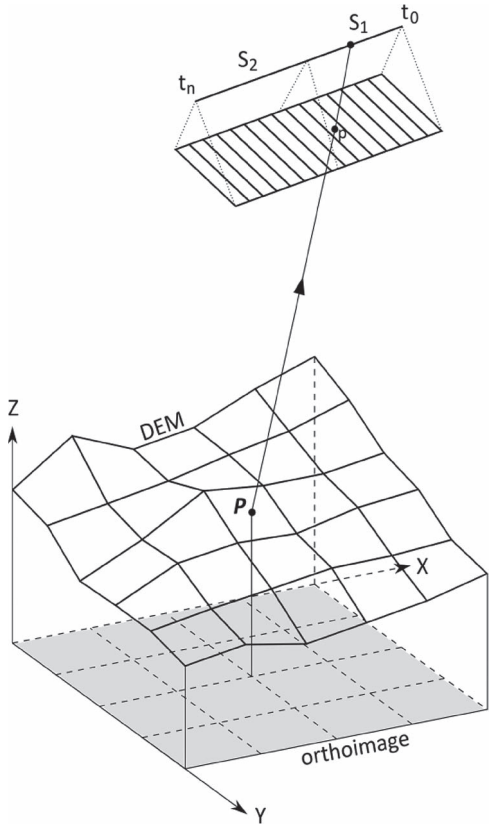

Fig. 5. Indirect orthorectification method was implemented in the chain. First, the corner coordinates of the orthoimage are computed. Then, for each pixel, the height value is extracted from the DEM (e.g., position P). The computed exterior orientation parameters determine the gray values (e.g., at the position of the point p) in the input image. In the process, the segment number (S_1 or S_2) and time of acquisition (from t_0 to t_n) must be taken into account. The pixel value in the orthoimage is determined by bilinear interpolation.

object space (orthoimage) and project the pixel onto the input image through the DEM. The gray value of the pixel is usually obtained with the resampling of the neighboring pixels on the input image. Indirect methods are generally better than direct ones in terms of quality and processing speed [30]. In addition, direct methods do not leave empty pixels, and therefore, no additional processing is needed. Despite all the advantages, indirectly generated orthoimages may contain errors if the input images have large viewing angles, the terrain is very rough, or a high-resolution DSM is utilized. In other cases (which are predominant), it is safe to use indirect methods. Due to the speed and ease of implementation, an indirect method is also used in the presented orthorectification algorithm.

The algorithm that was implemented in the chain is based on the research made by Kim *et al.* [30]. It was adapted to two segments and 24 exterior orientation parameters of the geometric model and works with any type of linear sensor image. The procedure was developed with a national DEM of Slovenia with a 12.5-m resolution, which is available for the whole country. The DEM's estimated height accuracy is 1.1 m on flat surfaces, 2.3 m on rolling hills areas, 3.8 m on hilly regions, and 7.0 m on mountains [31]. If a DEM with different characteristics (e.g., resolution) is required and available, it can be easily included.

TABLE I
CHARACTERISTICS OF THE RAPIDEYE IMAGES USED IN THE RESEARCH

Image	Date	Off-nadir angle (°)	Size (px)	Cloud cover (%)
Radgona	11.6.2011	3.65	11802×7604	0
Koper	18.8.2012	6.74	11796×10753	1
Bohinj	1.8.2013	0.12	11802×11223	3

III. METHODOLOGY AND RESULTS OF THE RESEARCH

A. Test Data and Research Methodology

The development of the production chain started with 19 RapidEye images that were acquired over Slovenia from 2011 to 2013. The procedure is currently functional and fully operational. Although it produces accurate results with all the available RapidEye images (covering all months from January to December with very different illumination and vegetation characteristics), this paper presents the empirical research obtained with three selected images that cover areas with different land covers and landforms and represent a good test polygon to demonstrate the performance of the developed automatic orthorectification chain (see Table I).

As presented in Table I, all the selected images were acquired during consecutive summers and show almost no clouds. The Bohinj image has an almost nadir, whereas the other two have small viewing angles. Due to the proximity of the state border, the Radgona image is smaller, with an area of approximately 3800 km^2, and the other two images have an area of around 5500 km^2. The images represent three morphologically different regions in Slovenia. The Koper image shows a coastal region with predominantly rolling hills. The Radgona area represents a predominantly flat terrain surrounded by hills. On the other hand, the Bohinj image was taken over a mountainous area with narrow valleys and high mountains. All three images contain areas of Slovenia and, in part, the neighboring countries.

The processing of the images follows the steps presented in Fig. 6.

Several tests were performed to verify the efficiency of the complete production chain and to compare the performance with different scenarios. Different blunder removal algorithms within the procedure were also compared. At the end, software robustness was checked with GCPs with manually added gross errors. Every image was submitted to the same tests. As the procedure is governed by a few main parameters (GCPs number, RANSAC iterations, and robust estimation method), only one parameter is tested at a time, and the others are taken as constants. Because RANSAC has a random component, the solution of the model is almost always slightly different. For this reason, all the tests with the RANSAC algorithm were conducted five times, and the results were averaged. The main tests are described in the following.

B. Results

1) Test on the Accuracy of Extracted GCPs: Before testing the geometric model, evaluation of automatically extracted

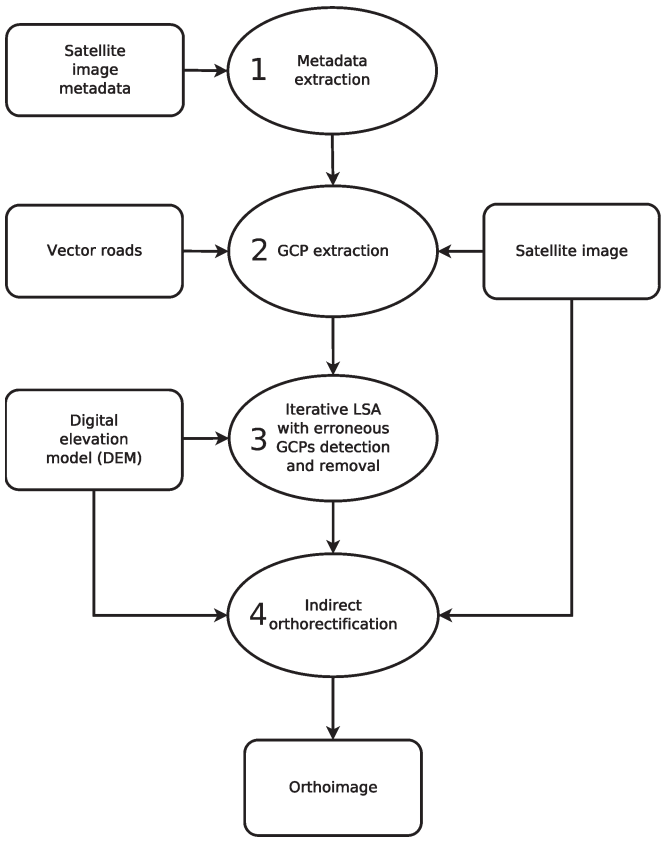

Fig. 6. Automatic orthorectification chain. The processing is divided into four main steps: metadata extraction, GCP extraction, iterative least squares adjustment with erroneous GCP detection and removal, and indirect orthorectification. The final result is the orthoimage.

points was performed. This test is simple and facilitates the understanding of the accuracy achieved using the model and the final accuracy of the orthoimages. The accuracy of the GCPs was obtained via the RPCs supplied by the vendor of the imagery and used as reference in this test. The manually measured and extracted GCP coordinates were compared with the computed bias-corrected coordinates using RPCs, and the results were analyzed. The accuracy (RMS error) is usually a good indicator of the automatic extraction process.

Before the accuracy check of the automatically generated GCPs, the RPCs were tested with manually selected and evenly distributed points, which were also used as independent check points (ICPs) in the least squares adjustment. In this manner, the quality of the supplied RPCs was checked, and the results were used to evaluate the tests with the automatically extracted GCPs. Although the RPCs are usually very accurate [22], their influence on the accuracy of the results is still questionable, particularly for images taken on rough terrain. The results with the manually selected GCPs are shown in Table II. If the error threshold of the measurements (about 0.5 pixels) is taken into account, the results show that the RPCs of the Radgona and Koper images are very accurate. As expected, the mountainous region of Bohinj has an RMS error larger than one pixel, which indicates RPCs with small errors. The maximum error values and the percentage of errors above 2σ confirm these findings.

TABLE II
ACCURACY OF THE MANUAL GCPS COMPARED WITH COORDINATES COMPUTED FROM RPCS

Image	Number of GCPs	Max error (px)	Errors over 2σ (%)	X RMS error (px)	Y RMS error (px)	Planar RMS error (px)
Radgona	22	1.15	0	0.45	0.49	0.66
Koper	26	1.61	0	0.37	0.86	0.94
Bohinj	27	2.26	7.4	0.75	0.90	1.17

TABLE III
ACCURACY OF THE AUTOMATICALLY EXTRACTED GCPS COMPARED WITH COORDINATES COMPUTED FROM RPCS

Image	Set	Number of GCPs	Max error (px)	Errors over 2σ (%)	X RMS error (px)	Y RMS error (px)	Planar RMS error (px)
Radgona	Large	501	5.86	1.6	0.51	0.41	0.65
	Small	50	5.68	4.0	0.79	0.55	0.96
Koper	Large	467	3.46	3.9	0.48	0.73	0.88
	Small	56	1.70	5.3	0.47	0.77	0.90
Bohinj	Large	325	3.63	4.3	0.75	1.24	1.45
	Small	53	3.02	5.7	0.69	1.08	1.28

The automatically extracted GCPs were checked against the same RPCs. For every image, two scenarios are presented, where the first one uses all points (large set) and the second one a decimated (small) set with about 50 points. In the second set, the points are selected based on their quality and distribution on the image. In Table III, the RMS errors of the automatically extracted GCPs are presented. In addition, the results of the extracted GCPs show a generally good consistency with the bias-corrected RPC coefficients. The RMS error is less than a pixel for the Radgona and Koper images and more than a pixel for the Bohinj region.

2) Test on Different Numbers of Used GCPs: Every image was divided into 100 tiles, and in every tile, the extraction of seven GCPs was attempted. These values were selected based on previous empirical tests that attempted to determine the maximum number of significant GCPs for RapidEye images. Because of the lack of roads in some tiles, type of terrain, and a few false detections, the number of points for every scene was different. The obtained number of GCPs was then considered the maximum number of GCPs to be tested. For every image, various sets of GCPs were generated by decimating the initial set considering the point quality and even distribution of the points in the image. Every set had a different number of points ranging from 500 to 15. Each set was used in the geometric model that worked with 100 RANSAC iterations and the Klein robust estimation method. RANSAC iterations continued until at least 90% of GCPs remained in the set.

The test results for all the images are listed in Table IV. It can be noted that the number of GCPs used in the final set is considerably reduced. The weak points were removed by RANSAC iterations, which assume that at least 90% of the points do not have gross errors or that the errors are small. The remaining points are further treated by robust estimation.

After the adjustment, the RMS errors are computed from the difference between the measured coordinates and the coordinates obtained with the geometric model results. The

TABLE IV
ACCURACY OF THE ADJUSTMENT RESULTS OBTAINED WITH DIFFERENT NUMBERS OF GCPS

Image	Number of GCPs	Number of used GCPs	Number of ICPs	GCP RMS error (px)	ICP RMS error (px)
Radgona	501	460	22	0.59	0.82
	303	273	22	0.62	0.85
	207	196	22	0.58	0.83
	96	87	22	0.65	0.87
	50	46	22	0.59	0.84
	32	32	22	0.82	0.87
	16	15	22	0.77	0.96
Koper	467	433	26	0.67	0.95
	295	276	26	0.70	0.86
	202	187	26	0.73	0.90
	98	92	26	0.71	0.96
	56	53	26	0.72	0.94
	32	31	26	0.69	1.01
	15	14	26	0.88	1.26
Bohinj	325	297	27	1.01	0.96
	203	184	27	1.01	0.99
	101	91	27	0.95	0.91
	53	48	27	0.94	1.17
	29	27	27	0.85	1.05
	16	15	27	0.80	0.97

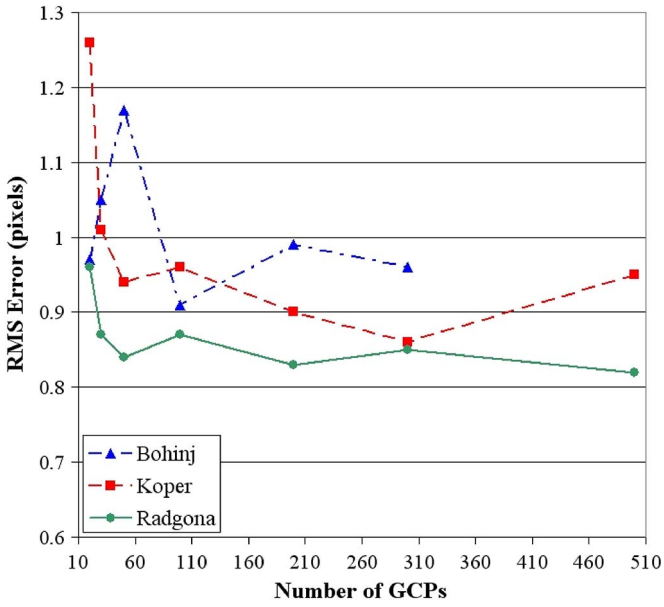

Fig. 7. RMS error at ICPs for every point set.

more significant RMS errors at ICPs that were manually measured are less than a pixel for almost every configuration (see Fig. 7).

3) Comparison of Different Robust Estimation Methods: Three robust estimation methods were tested: the Danish method, the method of Klein, and the hyperbolic function. We used the number of GCPs determined in the previous test. The test worked with 100 RANSAC iterations that continued until at least 90% of GCPs remained in the set.

Table V presents the RMS errors of the GCPs and the ICPs after the RANSAC iterations and at the end of the adjustment when the results are refined with robust estimation methods. From the results, it can be seen that robust estimation rarely

TABLE V
COMPARISON BETWEEN THE ROBUST ESTIMATION METHODS

Image	RANSAC (100 iter.) GCP RMS error (px)	RANSAC (100 iter.) ICP RMS error (px)	Method	Robust estimation GCP RMS error (px)	Robust estimation ICP RMS error (px)
Radgona	0.76	0.82	Danish	0.85	0.86
	0.66	0.83	Hyperbolic	0.66	0.83
	0.76	0.82	Klein	0.77	0.83
Koper	0.81	0.93	Danish	2.64	3.29
	0.75	0.87	Hyperbolic	0.71	0.84
	0.75	0.88	Klein	0.74	0.88
Bohinj	1.01	0.98	Danish	0.98	0.89
	0.97	0.94	Hyperbolic	0.97	0.94
	0.98	0.96	Klein	0.98	0.96

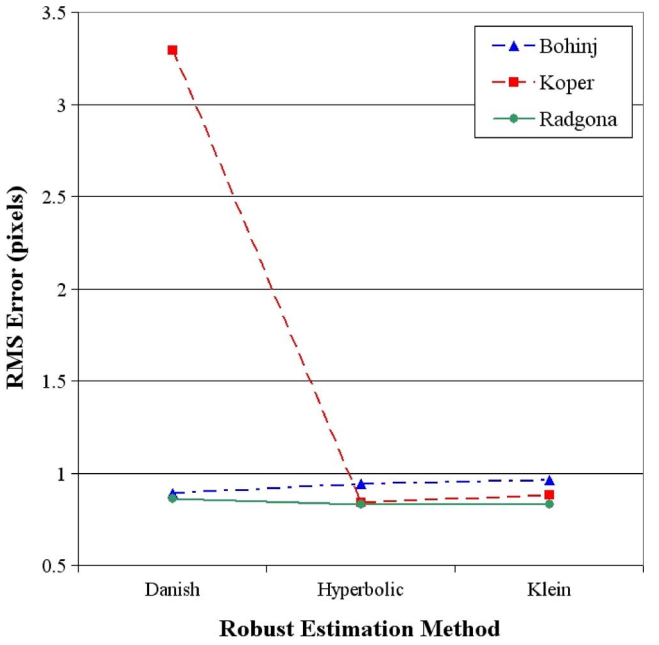

Fig. 8. Behavior of the tested robust estimation methods.

improves the results after the RANSAC-based adjustment. The results usually remain unchanged, which indicates a good performance of the iterative RANSAC method.

When comparing the robust estimation methods (see Fig. 8), it can be noted that the Danish method (using an exponential weight function) is not always reliable and sometimes produces large errors. The other two methods are based on the hyperbolic weight function and perform well.

4) Test on Gross Error Detection and Removal Methods: Performance of the model was tested with the introduction of artificial gross errors to GCPs. Two sets of points (large and small) were chosen for each image. In the large set, ten evenly distributed points with good quality were selected, and errors from one to ten pixels were added to both coordinates. In the small set, errors of one to five pixels were added to only five GCPs. The test operated with 100 RANSAC iterations and the Klein robust estimation method.

The adjustment results are presented in Tables VI and VII. In the Radgona test area, the RANSAC procedure removed 13 GCPs in the large set, where seven GCPs had artificial gross errors from four to ten pixels. Only three points with the lowest

TABLE VI
ADJUSTMENT RESULTS WITH THE NUMBER OF PRESENT (EP) AND REMOVED (ER) ERRONEOUS GCPS AND RMS ERRORS AFTER THE RANSAC ADJUSTMENT AND AT THE END (ROBUST ESTIMATION)

Image	Set	Number of GCPs	Number of used GCPs	Threshold (%)	ER/EP	RANSAC (100 iter.)		Robust estimation (Klein)	
						GCP RMS error (px)	ICP RMS error (px)	GCP RMS error (px)	ICP RMS error (px)
Radgona	Large	207	194	90	7/10	0.75	0.85	0.76	0.82
	Small	50	46	90	2/5	0.94	0.97	0.95	0.91
Koper	Large	202	187	90	6/10	0.95	0.95	0.88	0.86
	Small	56	52	90	3/5	0.92	0.99	0.85	1.01
Bohinj	Large	101	94	90	5/10	1.38	1.09	1.21	0.93
	Small	29	25	80	3/5	0.94	1.15	0.94	1.11

TABLE VII
RESIDUALS OF THE ERRONEOUS GCPS THAT REMAINED AFTER THE RANSAC ADJUSTMENT FOR THE LARGE AND SMALL SETS

Image	Gross error (px)	Large set		Small set	
		dx (px)	dy (px)	dx (px)	dy (px)
Radgona	1	0.05	1.07	-1.48	0.68
	2	-2.24	1.73	-1.96	1.49
	3	-3.34	2.98	-2.72	2.24
Koper	1	-1.11	1.09	-0.86	0.52
	2	-2.52	1.60	-2.52	1.09
	3	-3.91	2.39	-	-
	4	-3.52	3.29	-	-
Bohinj	1	-0.32	0.59	-1.69	1.07
	2	-2.07	2.28	-	-
	3	-2.78	2.44	-2.01	1.10
	4	-4.63	2.96	-	-
	5	-4.56	3.15	-	-

errors remained in the set, which were then treated with robust estimation. The accuracy of the final results is comparable with the one without the added errors (see Table IV). The results suggest that robust estimation generally improves the accuracy of the adjustment (see Fig. 9). Table VII presents the residuals of the erroneous points, which remained in the second part of the adjustment. The values are very similar to the errors added, which means that the geometric model excluded them and limited their influence on the results. In the Koper region, RANSAC left four GCPs with errors in the large set and only two in the small set (see Fig. 10). In this case, the final accuracy of the results is not affected by the introduced errors, and the residuals of the erroneous GCPs reflect the added gross errors. Although the results for the mountainous region of Bohinj are similar to the previous cases, some differences in the points removed were nevertheless observed.

5) Test on the Accuracy of Orthorectification: The orthoimages were generated with exterior orientation parameters from the most accurate results and a DEM with a 12.5-m resolution. The accuracy of the orthoimages was assessed with manually selected check points. Thirty points placed on road intersections were chosen all over each orthoimage. Coordinates of the same locations were taken from national aerial orthophoto images with a resolution of 0.5 m and an estimated accuracy of below 1 m. The comparison of the coordinates gave the orthorectification accuracy (RMS error).

Table VIII shows the positional accuracy (RMS error) achieved with check points that were manually measured on the reference image and RapidEye orthoimages. The resulting RMS errors at ICPs (see Fig. 11) indicate a high correlation with the results at ICPs after the adjustment (see Table IV).

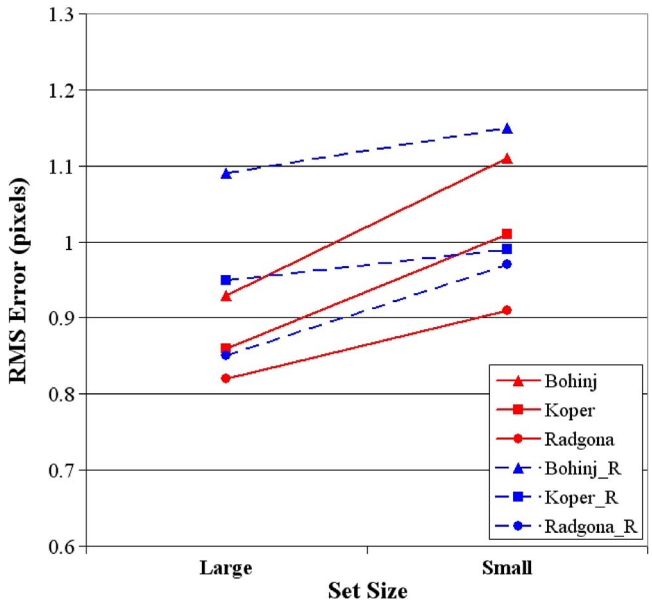

Fig. 9. Adjustment results (RMS error at ICPs) (dashed line) after RANSAC adjustment and (solid line) at the end for the large and small sets. It can be noted that robust estimation generally improves the accuracy of the adjustment.

C. Discussion

With the presented automatic extraction method, subpixel GCP positional accuracy can be achieved. The magnitude of the residuals of automatically extracted GCPs compared with RPCs is as expected if we take into account the topography of the regions, which also influences the RPCs. It is interesting to note that, in two cases, the smaller sets of points have slightly larger errors, which means that the quality point criterion is not completely reliable and that the selection of evenly distributed points also retains points with larger errors. For the validation of the orthorectification procedure, it is important to quantify the errors of the extracted GCPs. Good indicators for this are the maximum error value and the percentage of errors that are 2σ from the mean error value as they might indicate the presence of gross errors. As it can be noticed from the values in Table III, possible gross errors are detected in all point sets, but their share is very small, always below 6%. Although the indicators are

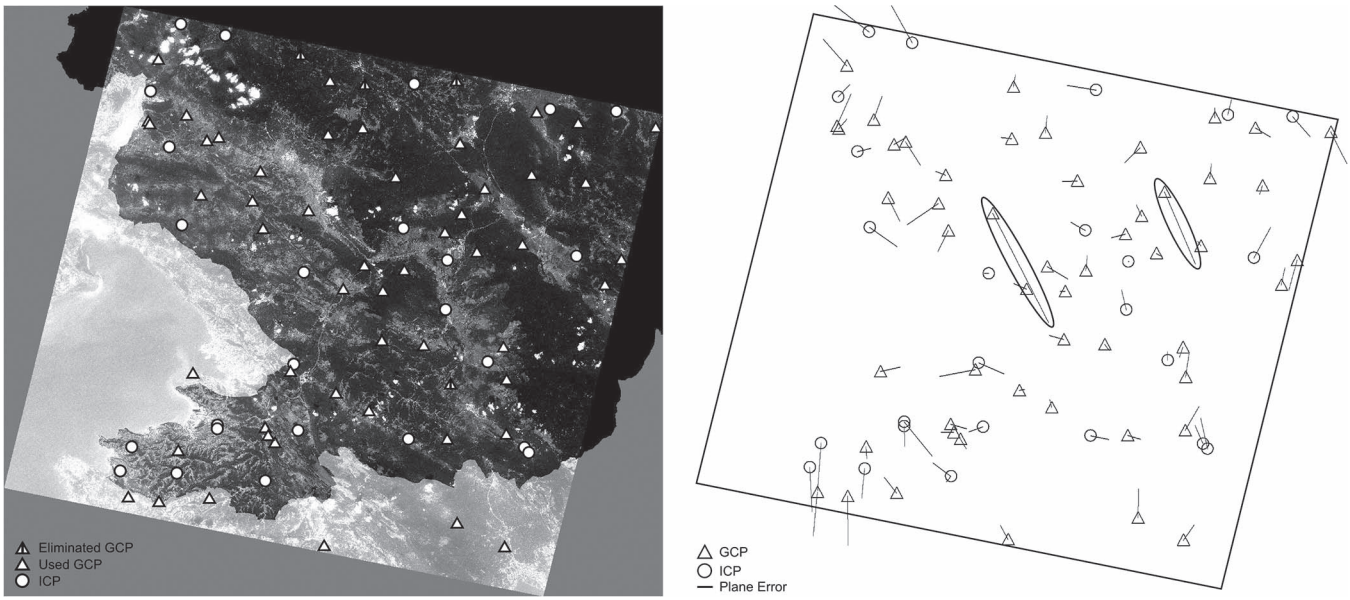

Fig. 10. GCP and ICP distribution and residuals. In the left image (Koper scene), Slovenian territory is represented in black color. GCPs are represented with triangles, and ICPs are in the form of circles. In the right image, two GCPs with artificial errors are marked with ellipses.

TABLE VIII
ACCURACY OF THE GENERATED ORTHOIMAGES COMPARED WITH THE NATIONAL AERIAL ORTHOPHOTO USED AS REFERENCE

Image	Number of ICPs	RMS error (px)		
		X	Y	Planar
Radgona	30	0.69	0.49	0.85
Koper	30	0.73	0.77	1.06
Bohinj	30	0.60	0.80	1.01

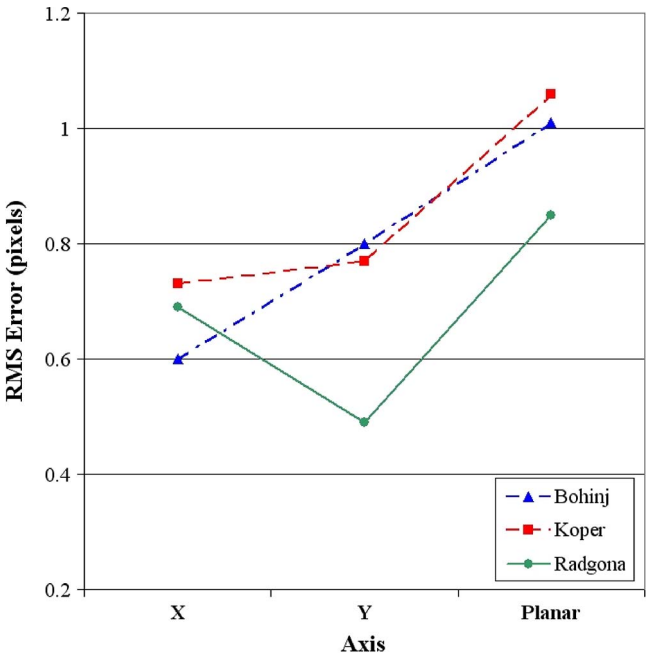

Fig. 11. RMS errors at 30 manually selected check points.

not completely reliable, it can be seen why good methods for gross error detection and removal had to be implemented in the geometric model.

After the geometric model computation, the RMS errors of the ICPs are generally below one pixel independent of the number of GCPs used in the adjustment. The values expectedly increase when a smaller number of points are used, but the difference between the sets is rather small. The results show that the model performs well also with a small number of GCPs. However, a greater number (around 100) of points produce better results and are preferable. With the automatization of the point extraction, a few hundred of points could be easily and quickly generated, and they do not significantly slow down the geometric model.

The choice of the robust estimation method is not trivial as some methods can produce unwanted results. The methods based on the hyperbolic weight function have proven to be good and robust. However, the results were improved only in the Koper test site. Some of our other results—not presented in this paper—suggest that the use of the robust estimation methods is necessary only when at least some gross errors are left in the processing after the first (RANSAC) part. It is therefore advisable to remove not more than 10% of GCPs also when more gross errors are present.

When gross errors were artificially introduced to the chosen GCPs, the geometric model (RANSAC) correctly removed most of them. The remaining points were iteratively excluded with the robust estimation method, which limited their influence on the final results. The same conclusions apply for the large and small sets. Small anomalies were found only in the mountainous region of Bohinj, where five points with gross errors remained in the final solution of the large set, which was composed of 101 GCPs. Their final residuals reflect the introduced error with some small deviations. Unexpected results appeared in the small set, where only the GCPs with one and three pixels of added errors were not removed in the first step. Additionally, the points show residuals with unusually low values. The reason is probably the small number of points

(only 29) and the rough terrain that affected the distribution of the GCPs. However, the accuracy after the adjustment is still comparable with the one without the added errors.

The accuracy of the orthoimages was manually verified with check points. The flat Radgona region gave the best accuracy (0.85 pixels), whereas the RMS error of the remaining regions is about one pixel (i.e., 6.5 m). It should be pointed out that the check points were measured only on well-defined road intersections, which were usually on low plain terrain. For this reason, the positional quality of the mountainous areas (central part of the Bohinj image) was not properly assessed.

The presented tests were undertaken to find the best processing methods and to make the complete procedure robust. The current version of the software works with one sensor-corrected image at a time. The computing takes about 1 h (depending on the image size) on a Xeon Quad-Core central processing unit at 2.5 GHz and 8 GB of random access memory. The metadata extraction step is almost instantaneous, whereas the GCP extraction takes about 38% of the time. For RapidEye images, the geometric model is usually fast, with 1%–2% of the overall processing time. The last step, i.e., orthorectification, is the most demanding and lasts the remaining 60%. Although the desired processing time was reached, the whole procedure can be still optimized with smart programming and distributed computing.

IV. Conclusion

A novel completely automatic orthorectification chain has been developed to precisely position optical satellite images. The chain uses automatically extracted GCPs from vector roads—a set of very stable and prominent features, which is globally available. A general physical geometric model with gross error detection and removal algorithms is implemented to compute exterior orientation parameters. The orthoimages are generated with an indirect orthorectification method. The novelty of our method is that it connects different processing parts in an operational and robust automatic chain, which employs innovative procedures, particularly in GCP extraction and geometric modeling with gross error removal steps. All the processing for one typical image takes about 1 h, which is much faster than traditional (manual) methods.

The overall performance of the processing chain was tested with three RapidEye images from different regions in Slovenia. The accuracy tests demonstrated the capability to orthorectify optical satellite images within one pixel size also when less than 20 GCPs are used and several gross errors of different magnitudes are present. The testing was useful also to select the methods that can guarantee the robustness and generality of the procedure.

The proposed orthorectification chain is currently functional and operational for RapidEye images, regardless of the acquisition date and region. However, because of the unavailability of other DEMs and the specific coordinate system, the chain is currently confined to Slovenia and part of the neighboring countries. The produced high-resolution orthoimages have been proven to be useful in many nationwide applications (e.g., environmental monitoring and change detection).

Developments for other high-resolution and VHR optical images (WorldView-2, Pleiades, SPOT 6, and THEOS) are in progress, and the first results are very promising. The follow-up version of the chain will also include other coordinate systems and a full-frame sensor geometric model that will process images from the Slovenian small satellite.

Acknowledgment

The authors would like to thank Space-SI for the provided data and P. Pehani for his help and support in coding. The constructive comments and suggestions from anonymous reviewers have considerably improved this paper.

References

[1] D. Poli, "A rigorous model for spaceborne linear array sensors," *Photogramm. Eng. Remote Sens.*, vol. 73, no. 2, pp. 187–196, Feb. 2007.

[2] C. Devaraj and C. A. Shah, "Automated geometric correction of multispectral images from High Resolution CCD Camera (HRCC) on-board CBERS-2 and CBERS-2B," *ISPRS J. Photogramm. Remote Sens.*, vol. 89, pp. 13–24, Mar. 2014.

[3] F. Eugenio and F. Marques, "Automatic satellite image georeferencing using a contour-matching approach," *IEEE Trans. Geosci. Remote Sens.*, vol. 41, no. 12, pp. 2869–2880, Dec. 2003.

[4] M. Gianinetto and M. Scaioni, "Automated geometric correction of high-resolution pushbroom satellite data," *Photogramm. Eng. Remote Sens.*, vol. 74, pp. 107–116, Jan. 2008.

[5] S. Leprince, S. Barbot, F. Ayoub, and J. P. Avouac, "Automatic and precise orthorectification, coregistration, and subpixel correlation of satellite images, application to ground deformation measurements," *IEEE Trans. Geosci. Remote Sens.*, vol. 45, no. 6, pp. 1529–1558, Jun. 2007.

[6] C. Liu and P. Chen, "Automatic extraction of ground control regions and orthorectification of remote sensing imagery," *Opt. Exp.*, vol. 17, no. 10, pp. 7970–7984, May 2009.

[7] Y. W. Sheng and D. E. Alsdorf, "Automated georeferencing and orthorectification of Amazon basin-wide SAR mosaics using SRTM DEM data," *IEEE Trans. Geosci. Remote Sens.*, vol. 43, no. 8, pp. 1929–1940, Aug. 2005.

[8] E. T. Slonecker, B. Johnson, and J. McMahon, "Automated imagery orthorectification pilot," *J. Appl. Remote Sens.*, vol. 3, no. 1, pp. 33 552–33 568, Oct. 2009.

[9] G. Q. Zhou, "Near real-time orthorectification and mosaic of small UAV video flow for time-critical event response," *IEEE Trans. Geosci. Remote Sens.*, vol. 47, no. 3, pp. 739–747, Mar. 2009.

[10] T. Toutin, "Review paper: Geometric processing of remote sensing images: Models, algorithms and methods," *Int. J. Remote Sens.*, vol. 25, no. 10, pp. 1893–1924, 2004.

[11] C. V. Tao and Y. Hu, "A comprehensive study of the rational function model for photogrammetric processing," *Photogramm. Eng. Remote Sens.*, vol. 67, pp. 1347–1357, 2001.

[12] J. Oh and C. Lee, "Automated bias-compensation of rational polynomial coefficients of high resolution satellite imagery based on topographic maps," *ISPRS J. Photogramm. Remote Sens.*, vol. 100, pp. 14–22, Feb. 2015.

[13] W. Baarda, "A testing procedure for use in geodetic networks," *Netherlands Geodetic Commission, Publications Geodesy, New Series*, vol. 2, p. 97, 1968.

[14] K. Kubik, W. Weng, and P. Frederiksen, "Oh, grosserrors!" in *Proc. 15th ISPRS Congr., Comission III*, Rio de Janeiro, Brasil, 1984, vol. 25, pp. 278–289.

[15] K. Oštir *et al.*, "Development of an automatic near-real-time image processing chain for small satellites," in *Proc. Small Satellites Earth Observ.: Dig. 9th Int. Symp. Int. Academy Astronautics*, R. Sandau, H.-P. Röser, and A. Valenzuela, Eds., Berlin, Germany, 2013, pp. 225–228.

[16] S. C. O. Grocott *et al.*, "The NEMO-HD spacecraft with breadboard instrument test results," in *Proc. Small Satellites Earth Observ.: Dig. 9th Int. Symp. Int. Academy Astronaut.*, R. Sandau, H.-P. Röser, A. Valenzuela, Eds., Berlin, Germany, Apr. 8–12, 2013, pp. 97–100.

[17] G. Zhou, W. Chen, J. A. Kelmelis, and D. Zhang, "A comprehensive study on urban true orthorectification," *IEEE Trans. Geosci. Remote Sens.*, vol. 43, no. 9, pp. 2138–2147, Sep. 2005.

[18] K. Kraus, *Photogrammetry*. Köln, Germany: Dümmler, 2000, vol. 1.
[19] T. Tuytelaars and K. Mikolajczyk, "Local invariant feature detectors: A survey," *Found. Trends Comput. Graph. Vis.*, vol. 3, no. 3, pp. 177–280, Jan. 2008.
[20] A. A. Sima and S. J. Buckley, "Optimizing SIFT for matching of short wave infrared and visible wavelength images," *Remote Sens.*, vol. 5, no. 5, pp. 2037–2056, 2013.
[21] J. Zaletelj, U. Burnik, and J. F. Tasič, "Registration of satellite images based on road network map," in *Proc. 8th ISPA*, Trieste, Italy, Sep. 4–6, 2013, pp 49–53.
[22] J. Grodecki and G. Dial, "Block adjustment of high-resolution satellite images described by rational polynomials," *Photogramm. Eng. Remote Sens.*, vol. 69, pp. 59–68, 2003.
[23] P. D. Noerdlinger, "Atmospheric refraction effects in Earth remote sensing," *ISPRS J. Photogramm. Remote Sens.*, vol. 54, no. 5/6, pp. 360–373, Dec. 1999.
[24] M. A. Fischler and R. C. Bolles, "Random sample consensus: A paradigm for model fitting with applications to image analysis and automated cartography," *Commun. ACM*, vol. 24, no. 6, pp. 381–395, Jun. 1981.
[25] K. Kubik, D. Merchant, and T. Schenk, "Robust estimation in photogrammetry," *Photogramm. Eng. Remote Sens.*, vol. 53, no. 2, pp. 167–169, Feb. 1987.
[26] P. J. Huber, "Robust estimation of a location parameters," *Ann. Math. Statist.*, vol. 35, no. 1, pp. 73–101, 1964.
[27] H. Klein and W. Förstner, "Realization of automatic error detection in the block adjustment program PAT-M43 using robust estimators," in *Proc. 15th ISPRS Congr. Comission III*, Rio de Janeiro, Brasil, 1984, vol. 25, pp. 234–245.
[28] A. F. Habib, E.-M. Kim, and C.-J. Kim, "New methodologies for true orthophoto generation," *Photogramm. Eng. Remote Sens.*, vol. 73, no. 1, pp. 25–36, Jan. 2007.
[29] Y. Sheng, "Comparative evaluation of iterative and non-iterative methods to ground coordinate determination from single aerial images," *Comput. Geosci.*, vol. 30, no. 3, pp. 267–279, Apr. 2004.
[30] T. Kim, D. Shin, and Y.-R. Lee, "Development of a robust algorithm for transformation of a 3D object point onto a 2-D image point for linear pushbroom imagery," *Photogramm. Eng. Remote Sens.*, vol. 67, no. 4, pp. 449–452, Apr. 2001.
[31] "Central evidence of spatial metadata," prostor3.gov.si. [Accessed: Nov. 26, 2014]. [Online]. Available: http://prostor3.gov.si/cepp_ang/index.jsp

Aleš Marsetič received the B.S. degree in geodetic engineering from the University of Ljubljana, Ljubljana, Slovenia, in 2005. He is currently working toward the Ph.D. degree in geodetic engineering at the University of Ljubljana.

Since 2006, he has been a Senior Technical Research Assistant with the Research Centre of the Slovenian Academy of Sciences and Arts, Ljubljana. From 2010 to 2014, he was with the Remote Sensing Department, Slovenian Centre of Excellence for Space Sciences and Technologies Space-SI. He has expertise in the automatization of satellite data preprocessing and in the designing of small satellites and the development of their ground segment data processing algorithms. His main research interests are photogrammetric applications in satellite remote sensing. In addition to photogrammetry (orthorectification, digital surface model generation), his field of work also encompasses optical satellite imagery registration and processing, spatial analysis, and lidar.

Mr. Marsetič was a recipient of the First Place Award in the Third Mission Idea Contest for Micro/Nano Satellite Utilization in 2014.

Krištof Oštir received the B.S. degree in physics and the M.S. and Ph.D. degrees in remote sensing from the University of Ljubljana, Ljubljana, Slovenia in 1994, 1997, and 2000, respectively.

Since 2001, he has been an Assistant Professor of remote sensing with the University of Ljubljana. Since 2007, he has been also a Research Advisor with the Research Centre of the Slovenian Academy of Sciences and Arts, Ljubljana. Since 2010, he has been also the Head of remote sensing operations with the Slovenian Centre of Excellence for Space Sciences and Technologies Space-SI, Ljubljana. He has authored six books and over 130 scientific papers. His main research fields are optical and radar remote sensing and image processing. In particular, he has performed research in radar interferometry, digital elevation production, land use and land cover classification, postprocessing, and fuzzy classification. The applications of remote sensing range from hazard monitoring change detection, archaeological site analysis, to paleoenvironment and paleorelief modeling. He is active in the development of small satellites for Earth observation.

Dr. Oštir was a recipient of the Gold Award from the Research Centre of the Slovenian Academy of Sciences and Arts in 2011 and the First Place Award in the Third Mission Idea Contest for Micro/Nano Satellite Utilization in 2014.

Mojca Kosmatin Fras received the B.S. degree from the University of Ljubljana, Ljubljana, Slovenia, in 1985 and the Ph.D. degree in geodetic sciences from the Polytechnic University of Milan, Milan, Italy, in 2003.

She started her professional career as a Researcher in 1985, after receiving the B.S. degree. From 1994 to 2002, she was the Head of the Photogrammetry Department with the Geodetic Institute of Slovenia. Since 2003, she has been an Assistant Professor with the Faculty of Civil and Geodetic Engineering, University of Ljubljana, where she lectures on various graduate and postgraduate subjects in photogrammetry and remote sensing. She has contributed in some European projects and many developmental and research projects of national importance. She has authored or coauthored over 20 scientific articles and was the Editor of two proceedings of the International Archives of Photogrammetry and Remote Sensing. Her recent research interests include topographical data extraction from aerial and high-resolution satellite images, data quality management, and aerial laser scanning.

Dr. Kosmatin Fras has been an active member of the International Society for Photogrammetry and Remote Sensing (ISPRS) for over 15 years, chairing two working groups and organizing some international workshops. She was a recipient of the President's Citation at the XXI ISPRS Congress in Beijing, in 2008, for her contributions to the Technical Commission VI during the period 2004–2008.